G3 Genes | Genomes | Genetics

INVESTIGATION

APC/C^{FZR-1} Controls SAS-5 Levels To Regulate Centrosome Duplication in *Caenorhabditis elegans*

Jeffrey C. Medley, Lauren E. DeMeyer, Megan M. Kabara, and Mi Hye Song[1]
Department of Biological Sciences, Oakland University, Rochester, Michigan 48309
ORCID IDs: 0000-0002-0965-4233 (J.C.M.); 0000-0003-1277-6503 (L.E.D.); 0000-0002-7942-8039 (M.M.K.); 0000-0001-8326-6602 (M.H.S.)

ABSTRACT As the primary microtubule-organizing center, centrosomes play a key role in establishing mitotic bipolar spindles that secure correct transmission of genomic content. For the fidelity of cell division, centrosome number must be strictly controlled by duplicating only once per cell cycle. Proper levels of centrosome proteins are shown to be critical for normal centrosome number and function. Overexpressing core centrosome factors leads to extra centrosomes, while depleting these factors results in centrosome duplication failure. In this regard, protein turnover by the ubiquitin-proteasome system provides a vital mechanism for the regulation of centrosome protein levels. Here, we report that FZR-1, the *Caenorhabditis elegans* homolog of Cdh1/Hct1/Fzr, a coactivator of the anaphase promoting complex/cyclosome (APC/C), an E3 ubiquitin ligase, functions as a negative regulator of centrosome duplication in the *C. elegans* embryo. During mitotic cell division in the early embryo, FZR-1 is associated with centrosomes and enriched at nuclei. Loss of *fzr-1* function restores centrosome duplication and embryonic viability to the hypomorphic *zyg-1(it25)* mutant, in part, through elevated levels of SAS-5 at centrosomes. Our data suggest that the APC/C^{FZR-1} regulates SAS-5 levels by directly recognizing the conserved KEN-box motif, contributing to proper centrosome duplication. Together, our work shows that FZR-1 plays a conserved role in regulating centrosome duplication in *C. elegans*.

KEYWORDS
FZR-1
C. elegans
Centrosome
E3 ubiquitin ligase
SAS-5

The centrosome is a small, nonmembranous organelle that serves as the primary microtubule-organizing center in animal cells. Each centrosome consists of a pair of barrel-shaped centrioles that are surrounded by a network of proteins called pericentriolar material (PCM). During mitosis, two centrosomes organize bipolar spindles that segregate genomic content equally into two daughter cells. Thus, tight control of centrosome number is vital for the maintenance of genomic integrity during cell division, by restricting centrosome duplication to once, and only once, per cell cycle. Erroneous centrosome duplication results in aberrant centrosome number that leads to chromosome missegregation and abnormal cell proliferation, and is associated with human disorders including cancers and microcephaly (Nigg and Stearns 2011; Gönczy 2015).

In the nematode *Caenorhabditis elegans*, extensive studies identified a set of core centrosome factors that are absolutely essential for centrosome duplication: the protein kinase ZYG-1 and the coiled-coil proteins SPD2, SAS-4, SAS-5, and SAS-6 (O'Connell *et al.* 2001; Kirkham *et al.* 2003; Leidel and Gönczy 2003; Dammermann *et al.* 2004; Delattre *et al.* 2004; Kemp *et al.* 2004; Pelletier *et al.* 2004; Leidel *et al.* 2005). SPD-2 and ZYG-1 localize early to the site of centriole formation and are required for the recruitment of the SAS-5/SAS-6 complex that sequentially recruits SAS-4 to the centriole (Delattre *et al.* 2006; Pelletier *et al.* 2006). These key factors are also present in other animal systems, suggesting an evolutionary conservation in centrosome duplication. For instance, the human genome contains homologs of the five centrosome factors found in *C. elegans*, Cep192/SPD-2 (Zhu *et al.* 2008), Plk4/ZYG-1 (Habedanck *et al.* 2005), STIL/SAS-5 (Arquint *et al.* 2012), HsSAS-6/SAS-6 (Leidel *et al.* 2005) and CPAP/SAS-4 (Kleylein-Sohn *et al.* 2007; Tang *et al.* 2009), and all these factors are shown to play a critical role in centrosome biogenesis (Fu *et al.* 2015; Gönczy 2015). However, the recently identified core centriole factor, SAS-7, that acts upstream of SPD-2 during *C. elegans* centriole duplication has not been found outside of nematodes (Sugioka *et al.* 2017).

doi: https://doi.org/10.1534/g3.117.300260
Manuscript received September 11, 2017; accepted for publication October 11, 2017; published Early Online October 13, 2017.

Supplemental material is available online at www.g3journal.org/lookup/suppl/doi:10.1534/g3.117.300260/-/DC1.
[1]Corresponding author: Biological Sciences, Oakland University, 344 Dodge Hall, 201 Meadow Brook Rd., Rochester, MI 48309. E-mail: msong2@oakland.edu

Maintaining the proper levels of centrosome proteins is critical for normal centrosome number and function (Kleylein-Sohn *et al.* 2007; Strnad *et al.* 2007; Rogers *et al.* 2009; Tang *et al.* 2009, 2011; Holland *et al.* 2010; Brownlee *et al.* 2011; Puklowski *et al.* 2011; Song *et al.* 2011; Meghini *et al.* 2016; Levine *et al.* 2017). In light of this, protein turnover by proteolysis provides a key mechanism for regulating the abundance of centrosome factors. A mechanism regulating protein levels is their degradation by the 26S proteasome that catalyzes the proteolysis of polyubiquitinated substrates (Livneh *et al.* 2016). The anaphase promoting complex/cyclosome (APC/C) is a multi-subunit E3 ubiquitin ligase that targets substrates for degradation (Acquaviva and Pines 2006; Peters 2006; Chang and Barford 2014). The substrate specificity of the APC/C is directed through the sequential, cell-cycle-dependent activity of two coactivators, Cdc20/Fzy/FZY-1 (Hartwell and Smith 1985; Dawson *et al.* 1995; Kitagawa *et al.* 2002) and Cdh1/Fzr/Hct1/FZR-1 (Schwab *et al.* 1997; Sigrist and Lehner 1997; Visintin *et al.* 1997; Fay *et al.* 2002). During early mitosis, Cdc20 acts as coactivator of the APC/C, and Cdh1 functions as coactivator to modulate the APC/C-dependent events at late mitosis and in G1 (Irniger and Nasmyth 1997; Visintin *et al.* 1997; Fang *et al.* 1998; Prinz *et al.* 1998; Shirayama *et al.* 1998). Upregulated targets in Cdh1-deficient cells are shown to be associated with the genomic instability signature of human cancers, and show a high correlation with poor prognosis (Carter *et al.* 2006; García-Higuera *et al.* 2008). Furthermore, a mutation in SIL/STIL (a human homolog of SAS-5) linked to primary microcephaly (MCPH; Kumar *et al.* 2009) results in deletion of the Cdh1-dependent destruction motif (KEN-box), leading to deregulated accumulation of STIL protein and centrosome amplification (Arquint and Nigg 2014). In *Drosophila*, the APC/$C^{Fzr/Cdh1}$ directly interacts with Spd2 through KEN-box recognition and targets Spd2 for degradation (Meghini *et al.* 2016). Therefore, the APC/$C^{Cdh1/Fzr/Hct1}$ plays a critical role in regulating the levels of key centrosome duplication factors in mammalian cells and flies.

In *C. elegans*, FZR-1 has been shown to be required for fertility, cell cycle progression and cell proliferation during embryonic and post-embryonic development via synthetic interaction with *lin-35/Rb* (Fay *et al.* 2002; The *et al.* 2015). However, the role of FZR-1 in centrosome assembly has not been described. In this study, we molecularly identified *fzr-1* as a genetic suppressor of *zyg-1*. Our results suggest that APC/C^{FZR-1} negatively regulates centrosome duplication, in part, through proteasomal degradation of SAS-5 in a KEN-box dependent fashion. Therefore, FZR-1, the *C. elegans* homolog of Cdh1/Hct1/Fzr, plays a conserved role in centrosome duplication.

MATERIALS AND METHODS

C. elegans strains and genetics

A full list of *C. elegans* strains used in this study is listed in Supplemental Material, Table S1 in File S1. All strains were derived from the wild-type Bristol N2 strain using standard genetic methods (Brenner 1974; Church *et al.* 1995).

Strains were maintained on MYOB plates seeded with *Escherichia coli* OP50 and grown at 19° unless otherwise indicated. The *fzr-1*::*gfp*::*3xflag* construct containing 21.6 Kbp of the *fzr-1* 5′UTR and 6 Kbp of the *fzr-1* 3′UTR was acquired from TransgenOme (construct number: 7127141463160758 F11, Sarov *et al.* 2012), which was used to generate the transgenic line, MTU10, expressing C-terminal GFP-tagged FZR-1. For the generation of N-terminal GFP-tagged FZR-1 (OC190), we used Gateway cloning (Invitrogen, Carlsbad, CA) to generate the construct. Coding sequence of *fzr-1* was PCR amplified from the cDNA clone yk1338f2, and cloned into pDONR221 (Invitrogen) and then the resulting entry clone was recombined into pID3.01 (pMS9.3), which is driven by the *pie-1* promotor. The transgenes were introduced into worms by standard particle bombardment (Praitis *et al.* 2001). For embryonic viability and brood size assays, individual L4 animals were transferred to clean plates, and allowed to self-fertilize for 24 hr at the temperatures indicated. For brood size assays, this was repeated until animals no longer produced embryos. Progeny were allowed at least 24 hr to complete embryogenesis before counting the number of progeny. The *fzr-1(RNAi)* experiments were performed by RNAi soaking (Song *et al.* 2008). To produce dsRNA for RNAi soaking, we amplified a DNA template from the cDNA clone yk1338f2 using the primers 5′-ATGGATGAGCAACCGCC-3′ and 5′-GCACTGTACGTAAAAAGTGATC-3′ that contained a T7 promoter sequence at their 5′ ends. *In vitro* transcription was performed using the T7-MEGAscript kit (Thermo-Fisher, Hanover park, IL). L4 animals were soaked overnight in M9 buffer containing either 0.1–0.4 mg dsRNA/ml or no dsRNA (control).

Mapping and molecular identification of szy-14

Both *szy-14(bs31)* and *szy-14(bs38)* suppressors were previously mapped between *dpy-10* and *unc-4* on chromosome II as described in Kemp *et al.* (2007). As *szy-14(bs31)* appears be a stronger suppressor (Figure 1B and Table 1, Kemp *et al.* 2007), we chose to use *szy-14(bs31)* for further mapping. Because *szy-14* mutants show no embryonic lethality, we decided to use the suppression of the *zyg-1(it25)* embryonic lethality by the *szy-14(bs31)* mutation for phenotyping. For single-nucleotide polymorphism (SNP) mapping, we mated *zyg-1(it25) dpy-10(e128) szy-14(bs31) unc-4(e120)* hermaphrodites with Hawaiian CB4856 males as described in Song *et al.* (2008), and isolated a total of 104 independent Dpy-nonUnc recombinants from the F2 generation. After establishing homozygous recombinant lines, we screened for the *fzr-1(bs31)* presence using the suppression of the *zyg-1(it25)* lethality at 24° supplemented by reduced brood size phenotype (Fay *et al.* 2002). For each phenotyping, we used the following control strains in parallel to accurately score the suppression: *zyg-1(it25)*, *zyg-1(it25) dpy-10(e128)*, *zyg-1(it25) dpy-10(e128) szy-14(bs31) unc-4(e120)*, *zyg-1(it25) szy-14(bs31)*, and *zyg-1(it25) szy-14(bs31) unc-4(e120)*. After careful phenotype examination, we determined 27 (out of 104) of the Dpy-nonUnc recombinants contain the *fzr-1(bs31)* mutation, which restores the *zyg-1(it25)* embryonic lethality, and that 77 (out of 104) of the Dpy-nonUnc recombinants do not contain the *fzr-1(bs31)* mutation, causing no suppression of the *zyg-1* lethality. Through fine mapping, we narrowed down the *szy-14* locus to a region of 57 kb between 9621265 and 9678204 on chromosome II. Then, we continued to molecularly screen for the *szy-14* gene by sequencing several candidate genes (*nos-3*, *kin-15*, *kin-16*, *wee-1.1*, *wee-1.3*, and *fzr-1*) located within a 57-kb interval on chromosome II. For sequencing the *fzr-1* gene, we used the following primers: forward 5′-TCTTGTTTCTGGTGGAGGT-3′ and reverse 5′-ACACGATACTGATGCCCAA-3′ for the *bs31* suppressor, and forward 5′-ATGGATGAGCAGCAACCGCC-3′ and reverse 5′-CAAGCTTGAGCTGTTGG-3′ for the *bs38* suppressor. Purified PCR amplicons were sequenced and aligned to the ORF, ZK1307.6 to identify the nucleotide substitution.

CRISPR/CAS-9 mediated genome editing

For genome editing, we used the co-CRISPR technique as previously described in *C. elegans* (Arribere *et al.* 2014; Paix *et al.* 2015). In brief, we microinjected N2 and *zyg-1(it25)* animals using a mixture containing recombinant SpCas9 (Paix *et al.* 2015), crRNAs targeting *sas-5* and *dpy-10* at 0.4–0.8 μg/μl, tracrRNA at 12 μg/μl, and single-stranded

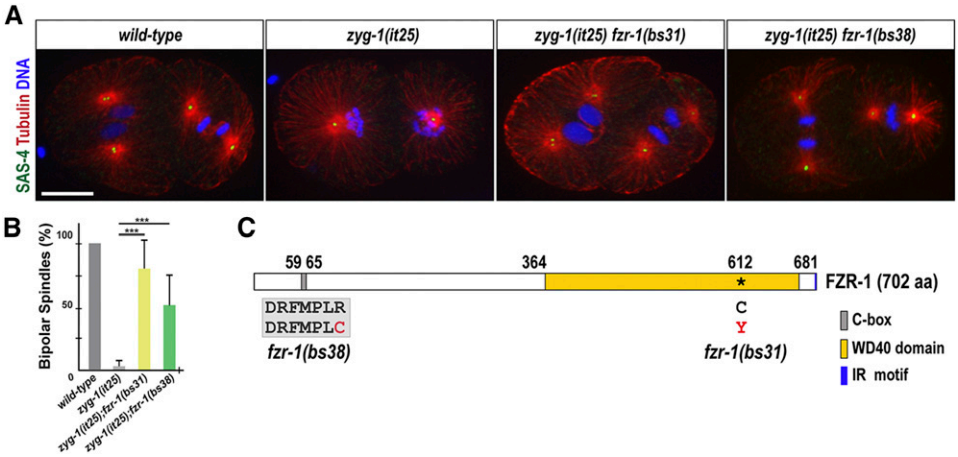

Figure 1 *fzr-1* mutations restore bipolar spindle formation to *zyg-1(it25)*. (A) Embryos grown at 24° stained for centrioles (SAS-4), microtubules, and DNA, illustrating mitotic spindles at the second mitosis. While the wild-type embryo (N2) forms bipolar spindles, the *zyg-1(it25)* mutant embryo exhibits monopolar spindles. However, bipolar spindle formation is restored in *zyg-1(it25) fzr-1(bs31)* and *zyg-1(it25) fzr-1(bs38)* double-mutant embryos. Bar, 10 μm. (B) Quantification of bipolar spindle formation during the second cell cycle. At the restrictive temperature (24°), wild-type (N2) embryos invariably assemble bipolar spindles (100% bipolar spindles, $n = 600$), whereas a great majority of *zyg-1(it25)* mutant embryos form monopolar spindles (3.3 ± 4.4% bipolar spindles, $n = 660$). In contrast, bipolar spindle formation is restored in *zyg-1(it25) fzr-1(bs31)* (79.9 ± 22.0% bipolar spindles, $n = 276$, $P < 0.001$) and *zyg-1(it25) fzr-1(bs38)* (51.4 ± 24.4%, $n = 404$, $P < 0.001$) double mutants. Average values are presented. Error bars represent SD. n is the number of blastomeres. *** $P < 0.001$ (two-tailed t-test). (C) Schematic of FZR-1 protein structure illustrates functional domains and the location of the missense mutations: R65C within the C-box in the *fzr-1(bs38)* mutant, and C612Y within WD40 domain in the *fzr-1(bs31)* mutant allele.

DNA oligonucleotides to repair *sas-5* and *dpy-10* at 25–100 ng/μl. Microinjection was performed using the XenoWorks microinjector (Sutter Instruments, Novato, CA) with a continuous pulse setting at 400–800 hPa. All RNA and DNA oligonucleotides used in this study were synthesized by Integrated DNA Technologies (IDT, Coralville, IA) and are listed in Table S2 in File S1. As we were unable to engineer a silent mutation into the PAM sequence used by the *sas-5* crRNA, we introduced six silent mutations to *sas-5* (aa 201–206; Figure 5A) by mutating 8 out of 20 the nucleotides that comprise the *sas-5* crRNA, in order to disrupt Cas9 recognition after homology-directed repair. After injection, animals were allowed to produce F1 progeny that were monitored for the presence of *dpy-10(cn64)*/+ rollers. To identify the *sas-5*$^{KEN\text{-}to\text{-}3A}$ mutation, we extracted genomic DNA from broods containing the highest frequency of F1 rollers. Using the primers, forward: 5′-TGCCCAAAATACGACAACG-3′ and reverse: 5′-TACACTACTCACGTCTGCT-3′, we amplified the region of *sas-5* containing the KEN-box sequence. As the repair template for the *sas-5*$^{KEN\text{-}to\text{-}3A}$ mutation introduces an *Hpy8*I restriction enzyme (NEB, Ipswich, MA) cutting site, we used an *Hpy8*I enzyme digestion to test for the introduction of our targeted mutation. After isolating homozygotes based on the *Hpy8*I cutting, we confirmed the *SAS-5*$^{KEN\text{-}to\text{-}3A}$ mutation by genomic DNA sequencing. Sequencing revealed that several lines were homozygous for the *SAS-5*$^{KEN\text{-}to\text{-}3A}$ mutation (Figure 5A and Table S1 in File S1). However, the strain MTU14, contained all of the silent mutations that we designed to disrupt Cas9 recognition without affecting the KEN-box (Figure 5A and Table S1 in File S1). Thus, we used MTU14 as a control for our assays.

Cytological analysis

To perform immunostaining, the following antibodies were used at 1:2000–3000 dilutions: α-Tubulin (DM1a; Sigma, St-Louis, MO), α-GFP: IgG$_1$κ (Roche, Indianapolis, IN), α-ZYG-1 (Stubenvoll *et al.* 2016), α-TBG-1(Stubenvoll *et al.* 2016), α-SAS-4 (Song *et al.* 2008), α-SAS-5 (Medley *et al.* 2017), and Alexa Fluor 488 and 561 (Invitrogen) as secondary antibodies. Confocal microscopy was performed as described (Stubenvoll *et al.* 2016) using a Nikon Eclipse Ti-U microscope equipped with a Plan Apo 60 × 1.4 NA lens, a Spinning Disk Confocal (CSU X1) and a Photometrics Evolve 512 camera. Images were acquired using MetaMorph software (Molecular Devices, Sunnyvale, CA). MetaMorph was used to draw and quantify regions of fluorescence intensity and Adobe Photoshop CS6 was used for image processing. To quantify centrosomal SAS-5 signals, the average intensity within an 8-pixel (1 pixel = 0.151 μm) diameter region was measured within an area centered on the centrosome and the focal plane with the highest average intensity was recorded. Centrosomal TBG-1 (γ-tubulin) levels were quantified in the same manner, except that a 25-pixel diameter region was used. For both SAS-5 and TBG-1 quantification, the average fluorescence intensity within a 25-pixel diameter region drawn outside of the embryo was used for background subtraction.

Immunoprecipitation (IP)

Embryos were collected from gravid worms using hypochlorite treatment (1:2:1 ratio of M9 buffer, 5.25% sodium hypochlorite, and 5 M NaCl), washed with M9 buffer five times and frozen in liquid nitrogen. Embryos were stored at −80° until use. IP experiment using α-GFP were performed following the protocol described previously (Stubenvoll *et al.* 2016); 20 μl of Mouse-α-GFP magnetic beads (MBL, Naka-ku, Nagoya, Japan) were used per reaction. The α-GFP beads were prepared by washing twice for 15 min in PBST (PBS; 0.1% Triton-X), followed by a third wash in 1× lysis buffer [50 mM HEPES, pH 7.4, 1 mM EDTA, 1 mM $MgCl_2$, 200 mM KCl, and 10% glycerol (v/v)] (Cheeseman *et al.* 2004). Embryos were suspended in 1× lysis buffer supplemented with complete protease inhibitor cocktail (Roche) and MG132 (Tocris, Avonmouth, Bristol, UK). The embryos were then milled for 3 min at 30 Hz using a Retsch MM 400 mixer-mill (Verder Scientific, Newtown, PA). Lysates were sonicated for 3 min in ice water using an ultrasonic bath (Thermo-Fisher). Samples were spun at 45,000 rpm for 45 min using a Sorvall RC M120EX ultracentrifuge (Thermo-Fisher). The supernatant was transferred to clean microcentrifuge tubes. Protein concentration was quantified using a NanoDrop spectrophotometer (Thermo-Fisher) and equivalent amount of total proteins was used for each reaction. Samples and α-GFP beads were incubated and rotated for 1 hr at 4°, and then washed five times for 5 min using PBST (PBS + 0.1% Triton-X 100). Samples were resuspended in 20 μl of a solution containing 2× Laemmli Sample

Table 1 Genetic analysis

	°C	% Embryonic Viability (Average ± SD)	*n* (Progeny)
N2	24	99.4 ± 0.7	1500
zyg-1(it25)		0 ± 7.2	1350
fzr-1(bs31)		96.8 ± 5.0	1200
zyg-1(it25) fzr-1(bs31)		44.5 ± 7.3	1273
zyg-1(it25) fzr-1(bs38)		28.6 ± 10.3	1004
zyg-1(it25) M9 buffer		0 ± 0	600
zyg-1(it25) fzr-1(RNAi)		10.7 ± 7.9	1045
zyg-1(or409) M9 buffer		0 ± 0	466
zyg-1(or409) fzr-1(RNAi)		2.2 ± 0	313
N2	24	100 ± 0	437
zyg-1(it25)		0 ± 0	1573
mat-3(or180)		0 ± 0	636
zyg-1(it25); mat-3(or180)		5.1 ± 1.2	1300
N2	24	100 ± 0	1143
sas-5$^{KEN\text{-}to\text{-}3A}$		99 ± 1.1	1386
zyg-1(it25); sas-5$^{KEN\text{-}to\text{-}KEN}$		0 ± 0	1165
zyg-1(it25); sas-5$^{KEN\text{-}to\text{-}3A}$		0 ± 0	1216
N2	22.5	100 ± 0	400
zyg-1(it25)		4.0 ± 5.4	1159
emb-1(hc57)		3.2 ± 2.1	1064
zyg-1(it25); emb-1(hc57)		3.3 ± 4.3	1337
N2	22.5	0 ± 0	817
sas-5$^{KEN\text{-}to\text{-}3A}$		0.1 ± 0.1	769
zyg-1(it25); sas-5$^{KEN\text{-}to\text{-}KEN}$		4.6 ± 4.0	1409
zyg-1(it25); sas-5$^{KEN\text{-}to\text{-}3A}$		35.3 ± 9.2	1341

Buffer (Sigma) and 10% β-mercaptoethanol (v/v), then boiled for 5 min. For protein input, 5 µl of embryonic lysates were diluted using 15 µl of a solution containing 2× Laemmli Sample Buffer and 10% β-mercaptoethanol (v/v), and boiled for 5 min before fractionating on a 4–12% NuPAGE Bis-Tris gel (Invitrogen).

Western blotting

For western blotting, samples were sonicated for 5 min and boiled in a solution of 2× Laemmli Sample Buffer and 10% β-mercaptoethanol before being fractionated on a 4–12% NuPAGE Bis-Tris gel (Invitrogen). The iBlot Gel Transfer system (Invitrogen) was then used to transfer samples to a nitrocellulose membrane. The following antibodies were used at 1:3000–10,000 dilutions: α-Tubulin: α-Tubulin (DM1a; Sigma), α-GFP: IgG$_1$κ (Roche), α-SAS-5 (Song *et al.* 2011), and α-TBG-1 (Stubenvoll *et al.* 2016). IRDye secondary antibodies (LI-COR Biosciences, Lincoln, NE) were used at a 1:10,000 dilution. Blots were imaged using the Odyssey infrared scanner (LI-COR Biosciences), and analyzed using Image Studio software (LI-COR Biosciences).

Statistical analysis

All *P*-values were calculated using two-tailed *t*-tests assuming equal variance among sample groups. Statistics are presented as Average ± SD unless otherwise specified. Data were independently replicated at least three times for all experiments and subsequently analyzed for statistical significance.

Data availability

All strains used in this study are available upon request. File S1 contains the following: Figure S1, Centrosome-associated TBG-1 levels are unaffected in *fzr-1(bs31)* and *sas-5$^{KEN\text{-}to\text{-}3A}$* mutant embryos; Figure S2, Brood size in *sas-5$^{KEN\text{-}to\text{-}3A}$* and *fzr-1(bs31)* mutants; Figure S3, SAS-5 levels are increased in *sas-5$^{KEN\text{-}to\text{-}3A}$* mutants; Table S1, List of strains used in this study; Table S2, List of oligonucleotides used for CRISPR/Cas9 genome editing.

RESULTS AND DISCUSSION

The szy-14 mutation restores centrosome duplication to zyg-1(it25) mutants

Through a genetic suppressor screen, the *szy-14* (suppressor of *zyg-1*) gene was originally identified that restores embryonic viability of the partial loss-of-function *zyg-1(it25)* mutant (Kemp *et al.* 2007). The *zyg-1(it25)* mutant embryo grown at the restrictive temperature (24°) fails to duplicate centrosomes during the first cell cycle, resulting in monopolar spindles at the second mitosis and 100% embryonic lethality (O'Connell *et al.* 2001). A complementation test identified two alleles, *szy-14(bs31)* and *szy-14(bs38)*, of the *szy-14* mutation that partially restore the embryonic viability of *zyg-1(it25)* but show slow growth phenotype without obvious cytological defects, indicating that the *szy-14* gene is not essential for embryonic viability (Table 1, Kemp *et al.* 2007).

Given that ZYG-1 is essential for proper centrosome duplication (O'Connell *et al.* 2001), we speculated that the *szy-14* mutation might suppress the embryonic lethality of *zyg-1(it25)* mutants via restoration of centrosome duplication. To examine centrosome duplication events, we quantified the percentage of bipolar spindles at the second mitosis, which indicates successful centrosome duplication during the first cell cycle (Figure 1, A and B). At the restrictive temperature 24°, both double mutant embryos, *zyg-1(it25); szy-14(bs31)* (79.9 ± 22.0%) and *zyg-1(it25); szy-14(bs38)* (51.4 ± 24.4%) produced bipolar spindles at a significantly higher rate, compared to *zyg-1(it25)* single mutant embryos (3.3 ± 4.4%) (Figure 1B). Our observation shows that the *szy-14* mutation restores centrosome duplication in *zyg-1(it25)* embryos, thereby restoring embryonic viability to *zyg-1(it25)* mutants.

Molecular identification of szy-14

The *szy-14* gene was initially mapped to the right arm of chromosome II between the morphological markers *dpy-10* and *unc-4* (Kemp *et al.* 2007). Using fine physical mapping, we located *szy-14* to an interval of 57 kb (ChrII: 9621265.. 9678204; Wormbase.org) that contains several known cell cycle regulators. Based on the genetic map position of the *szy-14* suppressor, we sequenced candidate genes within this interval to detect any mutations in *szy-14* mutants. Sequencing revealed that *szy-14(bs38)* mutants contain a single substitution (C-to-T) in exon 2, and *szy-14(bs31)* mutants carry a mutation (G-to-A) in exon 5 of the ORF ZK1307.6 that corresponds to the *fzr-1* gene. Consistently, inhibiting FZR-1 by RNAi soaking partially restores embryonic viability in both *zyg-1(it25)* and *zyg-1(or409)* mutant alleles (Table 1), indicating that loss-of-function of *fzr-1* leads to the restoration of embryonic viability to the *zyg-1* mutants. Together, we determined that the *bs31* and *bs38* mutations are alleles of the *fzr-1* gene. Hereafter, we refer to *szy-14(bs31)* and *szy-14(bs38)* mutants as *fzr-1(bs31)* and *fzr-1(bs38)* mutants, respectively.

fzr-1 encodes a conserved coactivator of the anaphase promoting complex/cyclosome (APC/C), the *C. elegans* homolog of Cdh1/Hct1/Fzr (Schwab *et al.* 1997; Sigrist and Lehner 1997; Visintin *et al.* 1997; Fay *et al.* 2002). The APC/C is an E3 ubiquitin ligase that orchestrates the sequential degradation of key cell cycle regulators during mitosis and early interphase (Song and Rape 2008). As part of this process, specific activators modulate the APC/C activity in different phases of mitosis. Specifically, FZR-1/Cdh1 modulates the APC/C at late mitosis and events in G1 during the time when centrosome duplication occurs.

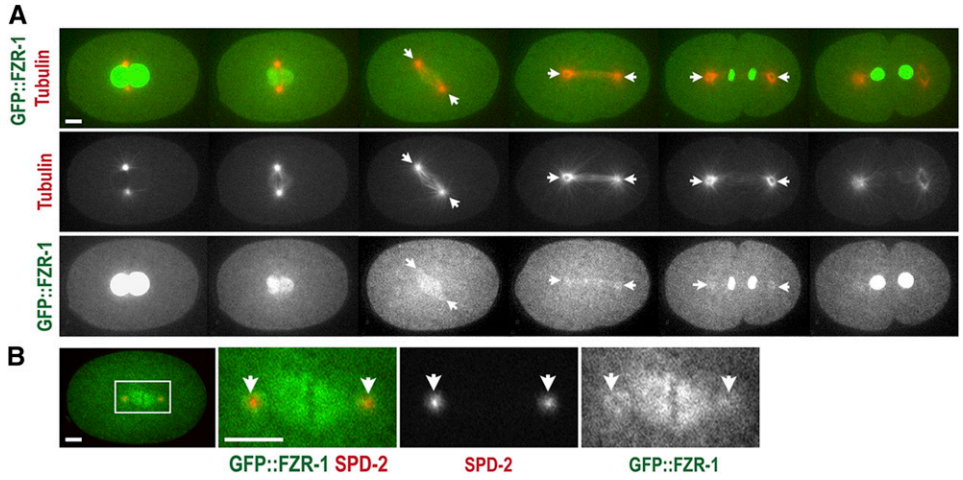

Figure 2 Subcellular localization of FZR-1 during the first cell cycle. (A) Still images from time-lapse movie of an embryo expressing GFP::FZR-1 and mCherry::tubulin. Movie was acquired at 1-min intervals. GFP::FZR-1 localizes at nuclei, mitotic spindles, and centrosomes (arrows). Expression of mCherry::tubulin used as a subcellular land-marker. (B) Embryo expressing GFP::FZR-1 and mCherry::SPD-2 displays that GFP::FZR-1 localizes to mitotic spindles and centrosomes (arrows) that colocalize with mCherry-SPD-2, a centrosome marker. Bar, 5 μm.

In each of the *fzr-1* mutant alleles, the single substitution leads to a missense mutation (Figure 1C). The *fzr-1(bs31)* mutation results in a missense mutation (C612Y) within the conserved WD40 repeat domain that is known to be involved in protein–protein interactions and is important for substrate recognition (Kraft *et al.* 2005; He *et al.* 2013). The *fzr-1(bs38)* mutation produces a missense mutation (R65C) at the conserved C-box of FZR-1. The C-box is known to be crucial for the physical interaction between FZR-1 and other APC/C subunits (Schwab *et al.* 2001; Thornton *et al.* 2006; Chang *et al.* 2015; Zhang *et al.* 2016). Thus, both *fzr-1(bs31)* and *fzr-1(bs38)* mutations appear to affect conserved domains that are critical for the function of the APC/C complex, suggesting that FZR-1 might regulate centrosome duplication through the APC/C complex.

FZR-1 localizes to nuclei and centrosomes during early cell division

To determine where FZR-1 might function during the early cell cycle, we produced two independent transgenic strains that express FZR-1 tagged with GFP at the N- or C-terminus (see *Materials and Methods*). To label microtubules, we mated GFP-tagged FZR-1 transgenic animals with the mCherry::β-tubulin expressing line, and performed 4D time-lapse movies to observe subcellular localization of GFP::FZR-1 throughout the first cell cycle (Figure 2A). Confocal imaging illustrates that during interphase and early mitosis, GFP::FZR-1 is highly enriched at the nuclei. After the nuclear envelope breaks down (NEBD), GFP::FZR-1 diffuses to the cytoplasm and reappears to the nuclei at late mitosis when the nuclear envelop reforms. After NEBD, GFP::FZR-1 becomes apparent at spindle microtubules, and centrosomes that colocalize with SPD-2, a centrosome protein (Figure 2B). Both GFP-tagged FZR-1 transgenic embryos exhibit similar subcellular distributions, except a slight difference in fluorescent intensity (data not shown). While we do not exclude the possibility that FZR-1 functions in the cytoplasm to regulate cellular levels of centrosome factors, our observations suggest that *C. elegans* FZR-1 might direct APC/C activity at centrosomes during late mitosis in early embryos, which is consistent with the role of FZR-1 as the coactivator of the APC/C at late mitosis in other organisms (Raff *et al.* 2002; Zhou *et al.* 2003; Meghini *et al.* 2016).

FZR-1 might function as a part of the APC/C complex to regulate centrosome duplication

Given that FZR-1 is a conserved coactivator of the APC/C, an E3 ubiquitin ligase, we hypothesized that FZR-1 functions as a part of the APC/C complex in centrosome assembly. If so, depleting other APC/C subunits should have a similar effect that loss of FZR-1 had on the *zyg-1(it25)* mutant. To examine how other core subunits of the APC/C complex might affect *zyg-1(it25)* mutants, we mated the *zyg-1(it25)* strain with *mat-3(or180)* mutants for the core APC8/CDC23 subunit (Golden *et al.* 2000), and *emb-1(hc57)* mutants for the conserved subunit APC16 in the *C. elegans* APC/C complex (Kops *et al.* 2010; Green *et al.* 2011; Shakes *et al.* 2011). By generating double homozygote mutants, we assayed for bipolar spindle formation and embryonic viability in *zyg-1(it25)*; *mat-3(or180)* and *zyg-1(it25)*; *emb-1(hc57)* double homozygous mutants (Figure 3 and Table 1). At the restrictive temperature 24°, *zyg-1(it25)*; *mat-3(or180)* double-mutant embryos exhibit a ninefold increase in bipolar spindle formation (81.8 ± 14.3%), compared to *zyg-1(it25)* single mutant embryos (9.1 ± 8.8%) during the second mitosis (Figure 3A). Consistently, 5% of *zyg-1(it25)*; *mat-3(or180)* double mutants produce viable progeny while 100% of *zyg-1(it25)* or *mat-3(or180)* single mutant progeny die at 24° (Table 1). In support of our results, the *mat-3(bs29)* allele has been reported as a genetic suppressor of *zyg-1* (Miller *et al.* 2016). This result also indicates that the *zyg-1(it25)* mutation partially restores embryonic viability of *mat-3(or180)* mutants, suggesting a mutual suppression between *zyg-1* and *mat-3*. Furthermore, we observed that the *emb-1* mutation suppresses the centrosome duplication phenotype of *zyg-1(it25)* mutants at the semi-restrictive temperature 22.5°. While 45.5 ± 11.9% of *zyg-1(it25)* embryos form bipolar spindles, 79.1 ± 12.4% of *zyg-1(it25)*; *emb-1(hc57)* double-mutant embryos produce bipolar spindles (Figure 3A). We, however, observed no significant restoration of embryonic viability in *zyg-1(it25)*; *emb-1(hc57)* double mutants (P = 0.691) compared to *zyg-1(it25)* single mutants (Table 1), presumably due to the strong embryonic lethality by the *emb-1(hc57)* mutation itself (Kops *et al.* 2010; Shakes *et al.* 2011). Our results indicate that loss of function mutations affecting the APC/C complex suppress the phenotype of *zyg-1(it25)* mutants. Therefore, FZR-1 might function as a component of the APC/C complex to regulate centrosome duplication in early *C. elegans* embryos.

Loss of FZR-1 results in elevated SAS-5 levels

Next, we wanted to understand how FZR-1 contributes to centrosome duplication. Since FZR-1 appears to function through the APC/C complex in centrosome assembly, we hypothesized that the APC/C^{FZR-1} specifically targets one or more centrosome regulators for ubiquitin-mediated degradation. If that is the case, depleting FZR-1 should protect substrates from degradation leading to accumulation of target proteins. To identify a direct substrate of APC/C^{FZR-1} that regulates

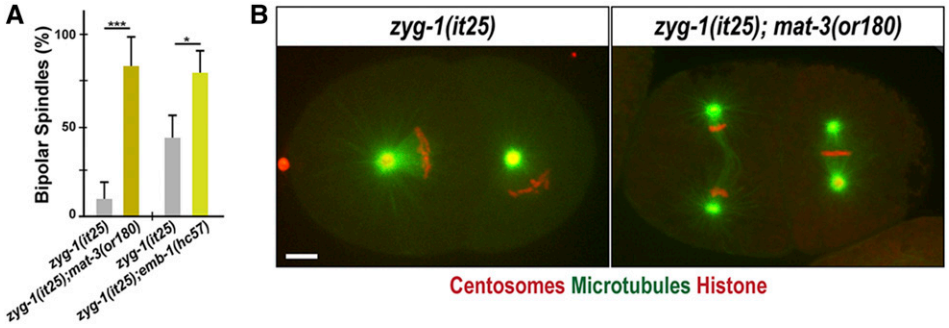

Figure 3 Inactivating the APC/C restores bipolar spindle formation to *zyg-1(it25)*. (A) Quantification of bipolar spindle formation during the second cell cycle. At 24°, *zyg-1(it25); mat-3(or180)* double mutants assembled bipolar spindles at a significantly higher percentage (81.8 ± 14.3%, n = 78, $P < 0.001$) than *zyg-1(it25)* embryos (9.1 ± 8.8%, n = 144). At 22.5°, there is an increase in bipolar spindle formation in *zyg-1(it25); emb-1(hc57)* double mutants (79.1 ± 12.4%, n = 228, $P = 0.03$), compared to *zyg-1(it25)* single mutants (45.5 ± 11.9%, n = 238). n is the number of blastomeres. * $P < 0.05$, *** $P < 0.001$ (two-tailed t-test). (B) Still images of embryos expressing GFP::β-tubulin, mCherry::γ-tubulin (centrosome marker) and mCherry::histone raised at 24° illustrate monopolar spindle formation in the *zyg-1(it25)* embryo, and bipolar spindle formation in the *zyg-1(it25); mat-3(or180)* double-mutant embryo. Bar, 5 μm.

centrosome assembly, we utilized the conserved FZR-1 coactivator specific recognition motif, KEN-box, to screen for a potential substrate (Glotzer *et al.* 1991; Pfleger and Kirschner 2000; Song and Rape 2011). The KEN-box appears to be the major degron motif that APC/C^{FZR-1} recognizes in centrosome duplication (Strnad *et al.* 2007; Tang *et al.* 2009; Arquint and Nigg 2014; Meghini *et al.* 2016). In human cells, HsSAS-6, STIL/SAS-5, and CPAP/SAS-4 contain a KEN-box motif, and APC/C$^{Cdh1/FZR-1}$ targets these proteins for ubiquitin-mediated proteolysis, thereby preventing extra centrosomes (Strnad *et al.* 2007; Tang *et al.* 2009; Arquint *et al.* 2012; Arquint and Nigg 2014). The *Drosophila* APC/C$^{Fzr/Cdh1/FZR-1}$ is also shown to target Spd2 for destruction through direct interaction with a KEN-box (Meghini *et al.* 2016). Interestingly in *C. elegans*, a putative KEN-box motif is present in SAS-5, but not in SAS-4 and SAS-6, which indicates an evolutionary divergence between humans and nematodes.

Protein stabilization by the *fzr-1* mutation might lead to increased levels of a centrosome-associated substrate, which may compensate for impaired ZYG-1 function at the centrosome. In *C. elegans*, SAS-5 is the only core centrosome duplication factor containing a KEN-box, which suggests SAS-5 as a potential target of the APC/C^{FZR-1}. If the APC/C^{FZR-1} targets SAS-5 directly through KEN-box for ubiquitin-mediated proteolysis, inhibiting FZR-1 should protect SAS-5 from degradation leading to SAS-5 accumulation. To examine how the *fzr-1* mutation affected SAS-5 stability, we immunostained embryos with anti-SAS-5, and quantified the fluorescence intensity of centrosome-associated SAS-5 (Figure 4, A and B). As ZYG-1 is required for SAS-5 localization to centrosomes, hyper-accumulation of SAS-5 might compensate for partial loss-of-function of ZYG-1, thereby restoring centrosome duplication to *zyg-1(it25)* mutants. In fact, our quantitative immunofluorescence revealed that *fzr-1(bs31)* embryos exhibit a significant increase (1.41 ± 0.42 fold; $P < 0.001$) in centrosomal SAS-5 levels at the first anaphase, compared to wild-type (Figure 4B). Consistently, compared to *zyg-1(it25)* single mutants, *zyg-1(it25); fzr-1(bs31)* double mutant embryos exhibit a 1.48-fold increase ($P < 0.001$) in centrosome-associated SAS-5 levels (Figure 4B). Indeed, centrosomal SAS-5 are restored to near wild-type levels in *zyg-1(it25); fzr-1(bs31)* double mutants (0.95 ± 0.44 fold; $P = 0.003$). We, however, observed no significant changes in centrosomal TBG-1 (γ-tubulin) levels in *fzr-1(bs31)* mutants (Figure S1 in File S1).

Elevated protein levels might influence centrosome-associated SAS-5 levels in *fzr-1(bs31)* mutants. To determine how inhibition of the APC/C^{FZR-1} affected overall protein levels, we performed quantitative western blot analysis using embryonic protein lysates and antibodies against centrosome proteins (Figure 4C). Our data indicate that *fzr-1(bs31)* embryos possess increased SAS-5 levels (~1.5-fold), relative to wild-type embryos, while the levels of SAS-6 and TBG-1 are not significantly affected in *fzr-1(bs31)* mutants (Figure 4C). Our observation on the SAS-6 levels in *fzr-1(bs31)* mutants is consistent with previous work by Miller *et al.* (2016), showing no increase in SAS-6 levels by the *mat-3(bs29)*/APC8 mutation that inhibits the APC/C function. These results suggest that *C. elegans* utilizes a different mechanism to control SAS-6 levels, unlike Human SAS-6, which is regulated by the APC/C-mediated proteolysis (Strnad *et al.* 2007). Furthermore, our immunoprecipitation suggests a physical interaction between SAS-5 and FZR-1 in *C. elegans* embryos (Figure 4D), supporting that SAS-5 might be a direct substrate of the APC/C^{FZR-1}. Consistent with our results in this study, prior study has shown that inhibiting the 26S proteasome leads to increased levels of SAS-5 (Song *et al.* 2011). Thus, SAS-5 levels are likely to be controlled through the ubiquitin-proteasome system.

Collectively, our data show that the *fzr-1* mutation leads to a significant increase in both cellular and centrosomal levels of SAS-5, suggesting that the APC/C^{FZR-1} might control SAS-5 levels via ubiquitin-mediated proteasomal degradation to regulate centrosome assembly in the *C. elegans* embryo.

Mutation of the KEN-box stabilizes SAS-5

If the APC/C^{FZR-1} directly targets substrates for destruction via the conserved KEN-box, mutating this motif should cause substantial resistance to ubiquitination-mediated degradation. To determine whether the APC/C^{FZR-1} targets SAS-5 through the KEN-box motif, we mutated the KEN-box at the endogenous *sas-5* locus. By using CRISPR/CAS-9 mediated genome editing (Paix *et al.* 2015), we generated mutant lines (*sas-5*$^{KEN\text{-}to\text{-}3A}$) carrying alanine substitutions of the SAS-5 KEN-box (Figure 5A). The *sas-5*$^{KEN\text{-}to\text{-}3A}$ mutant embryo exhibits no obvious cell cycle defects or embryonic lethality (Table 1), consistent with *fzr-1* mutants (Kemp *et al.* 2007). *sas-5*$^{KEN\text{-}to\text{-}3A}$ animals exhibit a slightly reduced (~80%) and irregular distribution of brood size within the population (Figure S2 in File S1). Reduced brood size and slow growth phenotypes were previously reported in *fzr-1* mutant alleles (Fay *et al.* 2002; Kemp *et al.* 2007).

Next, we asked how the *sas-5*$^{KEN\text{-}to\text{-}3A}$ mutation affected *zyg-1(it25)* mutants. If the APC/C^{FZR-1}-mediated proteolysis of SAS-5 accounts for the suppression of *zyg-1*, *sas-5*$^{KEN\text{-}to\text{-}3A}$ mutants should mimic the *fzr-1* mutation that suppresses *zyg-1* mutants. By mating the *sas-5*$^{KEN\text{-}to\text{-}3A}$ mutant with *zyg-1(it25)* animals, we tested whether the *sas-5*$^{KEN\text{-}to\text{-}3A}$ mutation could genetically suppress *zyg-1* mutants, by assaying for embryonic viability and centrosome duplication (Figure 5B and Table 1).

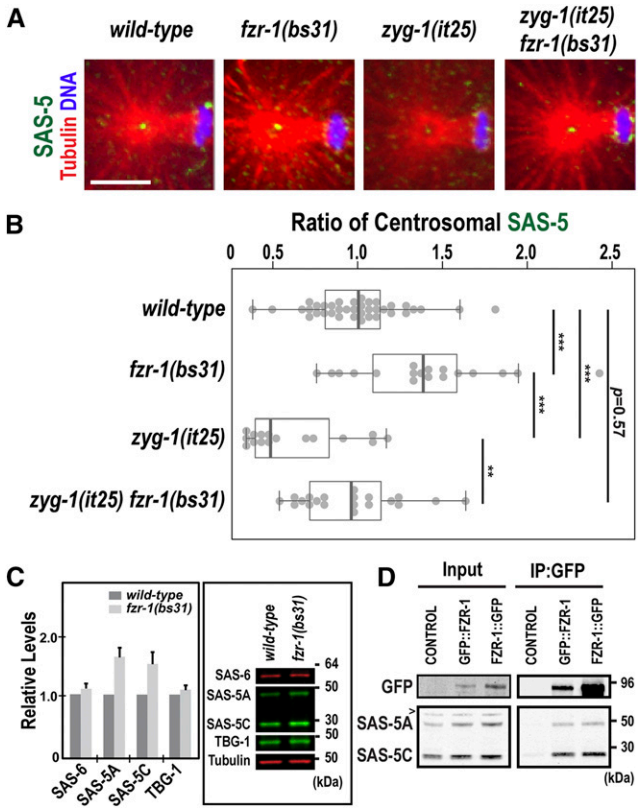

Figure 4 Loss of FZR-1 results in elevated SAS-5 levels. (A) Images of centrosomes stained for SAS-5 (green) at the first anaphase. Bar, 5 μm. (B) Quantification of centrosome-associated SAS-5 levels at the first anaphase. SAS-5 levels are normalized to the average fluorescence intensity in wild-type centrosomes. *fzr-1(bs31)* embryos exhibit increased levels of centrosomal SAS-5 (1.41 ± 0.42 fold, n = 18; $P < 0.001$) relative to wild-type controls (1.00 ± 0.28 fold, n = 38). In *zyg-1(it25) fzr-1(bs31)* double mutants, centrosomal SAS-5 levels are restored to near wild-type levels (0.95 ± 0.44-fold, n = 20; $P = 0.003$), compared to *zyg-1(it25)* embryos that show decreased levels of centrosomal SAS-5 (0.64 ± 0.28-fold, n = 16). n is the number of centrosomes. Each dot represents a centrosome. Box ranges from the first through third quartile of the data. Thick bar indicates the median. Solid gray line extends 1.5 times the interquartile range or to the minimum and maximum data point. ** $P < 0.01$, *** $P < 0.001$ (two-tailed t-test). (C) Quantitative western blot analyses show that (left panel) *fzr-1(bs31)* mutant embryos possess increased levels of both SAS-5 isoforms, SAS-5A (1.56 ± 0.16-fold) and SAS-5C (1.48 ± 0.19-fold), compared to wild-type (N2) embryos. However, there were no significant differences in levels of either SAS-6 (1.09 ± 0.08-fold) or TBG-1 (1.08 ± 0.07-fold) between *fzr-1(bs31)* mutant and wild-type embryos. Four biological samples and eight technical replicates were used. Average values are presented and error bars are SD. Right panel: Representative western blot using embryonic lysates from *fzr-1(bs31)* mutants and *N2* animals. Tubulin was used as a loading control. (D) IP using anti-GFP suggests that FZR-1 physically interacts with SAS-5. Both SAS-5 isoforms (SAS-5A, SAS-5C) coprecipitate with GFP::FZR-1 or FZR-1::GFP. Wild-type (N2) control embryos were used as a negative control of IP; ~1% of total embryonic lysates was loaded in the input lanes. > indicates a nonspecific detection by the SAS-5 antibody.

For the *zyg-1(it25)* mutant control in this experiment, we used the strain MTU14 [*zyg-1(it25)*; *sas-5*$^{KEN\text{-}to\text{-}KEN}$, Table S1 in File S1] that contains the equivalent modifications, except the KEN-box, to the *sas-5*$^{KEN\text{-}to\text{-}3A}$ mutation (Figure 5A, see *Materials and Methods*). At the semirestrictive temperature 22.5°, *zyg-1(it25)*; *sas-5*$^{KEN\text{-}to\text{-}3A}$ animals lead to a 7.7-fold increase in the frequency of viable progeny (35.3 ± 9.2%; $P < 0.0001$), compared to *zyg-1(it25)*; *sas-5*$^{KEN\text{-}to\text{-}KEN}$ mutant controls (4.6 ± 4.0%) (Table 1). Consistently, *zyg-1(it25)*; *sas-5*$^{KEN\text{-}to\text{-}3A}$ embryos exhibit successful bipolar spindle assembly at a significantly higher rate (67.5 ± 16.3%; $P = 0.02$) than *zyg-1(it25)*; *sas-5*$^{KEN\text{-}to\text{-}KEN}$ embryos (35.1 ± 10.7%) at the two-cell stage (Figure 5B). These results suggest that the *sas-5*$^{KEN\text{-}to\text{-}3A}$ mutation does partially restore embryonic viability and centrosome duplication to *zyg-1(it25)* mutants at 22.5°. However, at the restrictive temperature (24°), where the *fzr-1* mutation shows a strong suppression (Figure 1B and Table 1), both *zyg-1(it25)*; *sas-5*$^{KEN\text{-}to\text{-}3A}$ double mutants and *zyg-1(it25)*; *sas-5*$^{KEN\text{-}to\text{-}KEN}$ mutant animals result in 100% embryonic lethality (Table 1). *zyg-1(it25)*; *sas-5*$^{KEN\text{-}to\text{-}3A}$ embryos (14.7% bipolar, n = 68) grown at 24° show only minor effect on centrosome duplication compared to *zyg-1(it25)*; *sas-5*$^{KEN\text{-}to\text{-}KEN}$ control embryos (7.6% bipolar, n = 66). The data obtained at 24° reveal that the *sas-5*$^{KEN\text{-}to\text{-}3A}$ mutation results in much weaker suppression to *zyg-1(it25)* mutants than the *fzr-1* mutation, suggesting that the SAS-5 KEN-box mutation does not generate the equivalent impact that results from the *fzr-1* mutation. If SAS-5 is the only APC/C$^{FZR\text{-}1}$ substrate that contributes to the suppression of *zyg-1* mutants, the *fzr-1* or KEN-box mutation might influence SAS-5 stability differently. In this scenario, FZR-1 might target SAS-5 through KEN-box and additional recognition motifs (*e.g.*, D-box), causing a greater effect on SAS-5 stability than the KEN-box mutation alone. To examine how the KEN-box mutation affected SAS-5 stability, we measured the fluorescence intensity of SAS-5 at centrosomes by quantitative immunofluorescence (Figure 5, C and D). At 22.5°, where the *sas-5*$^{KEN\text{-}to\text{-}3A}$ mutation restores centrosome duplication and embryonic viability to *zyg-1(it25)*, *sas-5*$^{KEN\text{-}to\text{-}3A}$ mutants exhibit a significant increase in centrosome-associated SAS-5 levels (~1.5-fold, $P < 0.001$), compared to wild-type (Figure 5, C and D). Consistently, *zyg-1(it25)*; *sas-5*$^{KEN\text{-}to\text{-}3A}$ embryos display ~1.4-fold ($P = 0.002$) increased SAS-5 levels at centrosomes, compared to *zyg-1(it25)*; *sas-5*$^{KEN\text{-}to\text{-}KEN}$ control embryos that contain reduced centrosomal SAS-5 levels (Figure 5D). Notably, *zyg-1(it25)*; *sas-5*$^{KEN\text{-}to\text{-}3A}$ embryos exhibit centrosomal SAS-5 levels nearly equivalent (~0.97-fold) to those of wild-type embryos (Figure 5D). As a control, we also quantified centrosomal TBG-1 levels, but saw no changes between *sas-5*$^{KEN\text{-}to\text{-}3A}$ mutants and the wild type (Figure S1 in File S1). Furthermore, we examined overall SAS-5 levels by quantitative western blot, finding that relative to wild-type embryos, *sas-5*$^{KEN\text{-}to\text{-}3A}$ mutant embryos possess ~1.5-fold increased SAS-5 levels (Figure S3 in File S1). Together, our quantification data reveal that the *sas-5*$^{KEN\text{-}to\text{-}3A}$ or *fzr*-1 mutation leads to nearly equivalent fold change (~1.5-fold) in both cellular and centrosome-associated SAS-5 levels (Figure 4, B and C, Figure 5D, and Figure S3 in File S1). Together, these results suggest that APC/C$^{FZR\text{-}1}$ directly targets SAS-5 in a KEN-box-dependent manner to control SAS-5 turnover, and that SAS-5 stabilization by blocking proteolysis results in elevated SAS-5 levels at the centrosome, partially contributing to the suppression of the *zyg-1(it25)* mutation. In human cells, APC/C^{Cdh1} recognizes a KEN-box to regulate the levels of STIL, the homolog of *C. elegans* SAS-5, and STIL deleted of the KEN-box leads to accumulation of STIL protein, and centrosome amplification (Arquint and Nigg 2014). While we do not observe extra centrosomes by the SAS-5 KEN-box mutation, our data show that that APC/C$^{FZR\text{-}1}$ controls SAS-5 stability via the direct recognition of the conserved degron motif, KEN-box, to regulate centrosome duplication in *C. elegans* embryos, suggesting a conserved mechanism for regulating SAS-5 levels between humans and nematodes.

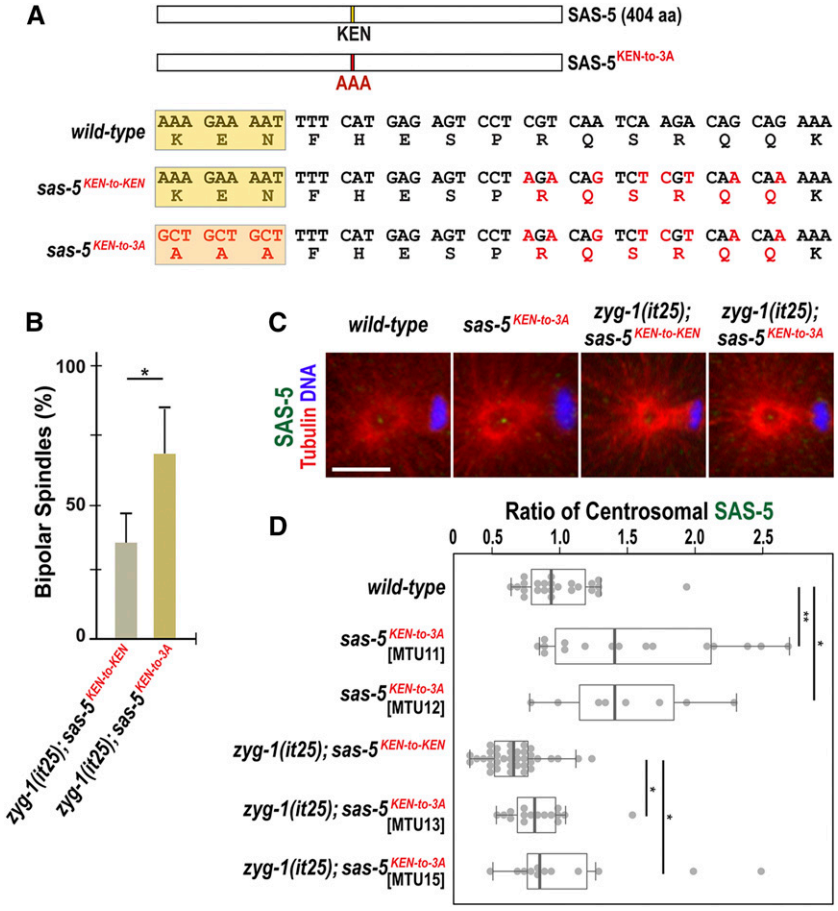

Figure 5 Mutation of the SAS-5 KEN-box leads to increased SAS-5 levels at centrosomes and restores centrosome duplication to *zyg-1(it25)* mutants. (A) SAS-5 contains a KEN-box (aa 213–216) motif. Mutations (red) are introduced at multiple sites to make alanine substitutions (AAA; 3A) for the KEN-box and additional silent mutations for the CRISPR genome editing (see *Materials and Methods*). The KEN-box is highlighted in yellow. Note that the *sas-5*$^{KEN\text{-}to\text{-}KEN}$ mutation contains the wild-type SAS-5 protein. (B) Quantification of bipolar spindle formation during the second cell cycle in *zyg-1(it25)*; *sas-5*$^{KEN\text{-}to\text{-}KEN}$ and *zyg-1(it25)*; *sas-5*$^{KEN\text{-}to\text{-}3A}$ embryos at 22.5°. *zyg-1(it25)*; *sas-5*$^{KEN\text{-}to\text{-}3A}$ double mutant embryos produce bipolar spindles at a higher rate (67.5 ± 16.3%, n = 124, P = 0.02) than *zyg-1(it25)*; *sas-5*$^{KEN\text{-}to\text{-}KEN}$ controls (35.1 ± 10.7%, n = 164). n is the number of blastomeres. Average values are presented and error bars are SD. (C) Centrosomes stained for SAS-5 (green) during the first anaphase. Bar, 5 μm. (D) Quantification of centrosomal SAS-5 levels during the first anaphase. We used two independently generated *sas-5*$^{KEN\text{-}to\text{-}3A}$ mutant lines to quantify SAS-5 levels (MTU11 and 12, Table S1 in File S1). SAS-5 levels at centrosomes are normalized to the average fluorescence intensity in wild-type centrosmes. Mutating the SAS-5 KEN-box leads to increased levels of centrosomal SAS-5 in both MTU11 (1.54 ± 0.63-fold, n = 16; P = 0.04) and MTU12 (1.48 ± 0.50 fold, n = 8; P = 0.03), compared to wild type (1.00 ± 0.29-fold; n = 24). Consistently, there are a significant increase in centrosomal SAS-5 levels in both *zyg-1(it25)*; *sas-5*$^{KEN\text{-}to\text{-}3A}$ double mutant lines (MTU13: 0.85 ± 0.24-fold, n = 16; P = 0.01 and MTU15: 1.09 ± 0.59-fold; n = 12; P = 0.03), compared to *zyg-1(it25)*; *sas-5*$^{KEN\text{-}to\text{-}KEN}$ control that contains reduced levels of centrosomal SAS-5 (0.67 ± 0.20-fold; n = 36). n is the number of centrosomes. Each dot represents a centrosome. Box ranges from the first through third quartile of the data. Thick bar indicates the median. Solid gray line extends 1.5 times the interquartile range, or to the minimum and maximum data point. * $P < 0.05$, ** $P < 0.01$ (two-tailed t-test).

Interestingly, although either inhibiting FZR-1 or mutating KEN-box influences SAS-5 stability at a comparable level, we observe a notable difference in the suppression level by these two mutations. Weaker suppression by the *sas-5*$^{KEN\text{-}to\text{-}3A}$ mutation suggests that the APC/C$^{FZR\text{-}1}$ might target additional substrates that cooperatively support the *zyg*-1 suppression. In this scenario, APC/C$^{FZR\text{-}1}$ might target other centrosome proteins outside core duplication factors through the conserved degron motifs, such as destruction (D)-box and KEN-box (Glotzer *et al.* 1991; Pfleger and Kirschner 2000). Alternatively, APC/C$^{FZR\text{-}1}$ might target additional core centrosome factors through other recognition motifs other than KEN-box, such as D-box (Glotzer *et al.* 1991) or unknown motif in the *C. elegans* system. In humans and flies, APC/C$^{Cdh1/Fzr}$ has been shown to regulate the levels of STIL/SAS-5, Spd2, HsSAS-6, and CPAP/SAS-4 (Strnad *et al.* 2007; Tang *et al.* 2009; Arquint and Nigg 2014; Meghini *et al.* 2016). While *C. elegans* homologs of these factors, except SAS-5, lack a KEN-box, all five centrosome proteins contain at least one putative D-box. An intriguing possibility, given the strong genetic interaction observed between *fzr-1* and *zyg-1*, is that ZYG-1 could be a novel substrate of APC/C$^{FZR\text{-}1}$. Additional work will be required to understand the complete mechanism of APC/C$^{FZR\text{-}1}$- dependent regulation of centrosome duplication in *C. elegans*. In summary, our study shows the APC/C$^{FZR\text{-}1}$-dependent proteolysis of SAS-5 partially contributes to the suppression of the *zyg*-1 mutants, and we report that FZR-1 functions as a negative regulator of centrosome duplication in *C. elegans*.

ACKNOWLEDGMENTS

We thank members of the Song laboratory (Naomi Haque, Brittany Rettig, Karina Saiyad and Michael Stubenvoll) for technical support and Kevin O'Connell and Andy Golden for RNAi and worm stains. We especially thank WormBase and the *Caenorhabditis* Genetics Center (CGC). WormBase is supported by grant U41 HG002223 from the National Human Genome Research Institute at the United States National Institutes of Health, the United Kingdom (UK) Medical Research Council and the UK Biotechnology and Biological Sciences Research Council. The CGC (St. Paul, MN), is funded by the National Institutes of Health Office of Research Infrastructure Programs (P40 OD010440). This work was supported by a grant [7R15GM11016-02 to M.H.S.] from the National Institute of General Medical Sciences, and Research Excellence Fund (to M.H.S.) from the Center for Biomedical Research at Oakland University. The funders had no role in study design, data collection and analysis, decision to publish, or preparation of the manuscript. No competing interests are declared.
Author contributions: J.C.M. and M.H.S. designed the experiments and wrote the manuscript. J.C.M. and M.H.S. performed quantifications of confocal imaging and protein levels from western blots.

J.C.M., L.E.D., M.M.K., and M.H.S. performed experiments and provided data.

LITERATURE CITED

Acquaviva, C., and J. Pines, 2006 The anaphase-promoting complex/cyclosome: APC/C. J. Cell Sci. 119: 2401–2404.

Arquint, C., and E. A. Nigg, 2014 STIL microcephaly mutations interfere with APC/C-mediated degradation and cause centriole amplification. Curr. Biol. 24: 351–360.

Arquint, C., K. F. Sonnen, Y. D. Stierhof, and E. A. Nigg, 2012 Cell-cycle-regulated expression of STIL controls centriole number in human cells. J. Cell Sci. 125: 1342–1352.

Arribere, J. A., R. T. Bell, B. X. Fu, K. L. Artiles, P. S. Hartman *et al.*, 2014 Efficient marker-free recovery of custom genetic modifications with CRISPR/Cas9 in *Caenorhabditis elegans*. Genetics 198: 837–846.

Brenner, S., 1974 The genetics of *Caenorhabditis elegans*. Genetics 77: 71–94.

Brownlee, C. W., J. E. Klebba, D. W. Buster, and G. C. Rogers, 2011 The protein phosphatase 2A regulatory subunit twins stabilizes Plk4 to induce centriole amplification. J. Cell Biol. 195: 231–243.

Carter, S. L., A. C. Eklund, I. S. Kohane, L. N. Harris, and Z. Szallasi, 2006 A signature of chromosomal instability inferred from gene expression profiles predicts clinical outcome in multiple human cancers. Nat. Genet. 38: 1043–1048.

Chang, L., and D. Barford, 2014 Insights into the anaphase-promoting complex: a molecular machine that regulates mitosis. Curr. Opin. Struct. Biol. 29: 1–9.

Chang, L., Z. Zhang, J. Yang, S. H. McLaughlin, and D. Barford, 2015 Atomic structure of the APC/C and its mechanism of protein ubiquitination. Nature 522: 450–454.

Cheeseman, I. M., S. Niessen, S. Anderson, F. Hyndman, J. R. Yates, III *et al.*, 2004 A conserved protein network controls assembly of the outer kinetochore and its ability to sustain tension. Genes Dev. 18: 2255–2268.

Church, D. L., K. L. Guan, and E. J. Lambie, 1995 Three genes of the MAP kinase cascade, *mek-2*, *mpk-1/sur-1 and let-60 ras*, are required for meiotic cell cycle progression in *Caenorhabditis elegans*. Development 121: 2525–2535.

Dammermann, A., T. Müller-Reichert, L. Pelletier, B. Habermann, A. Desai *et al.*, 2004 Centriole assembly requires both centriolar and pericentriolar material proteins. Dev. Cell 7: 815–829.

Dawson, I. A., S. Roth, and S. Artavanis-Tsakonas, 1995 The *Drosophila* cell cycle gene *fizzy* is required for normal degradation of cyclins A and B during mitosis and has homology to the CDC20 gene of *Saccharomyces cerevisiae*. J. Cell Biol. 129: 725–737.

Delattre, M., S. Leidel, K. Wani, K. Baumer, J. Bamat *et al.*, 2004 Centriolar SAS-5 is required for centrosome duplication in *C. elegans*. Nat. Cell Biol. 6: 656–664.

Delattre, M., C. Canard, and P. Gönczy, 2006 Sequential protein recruitment in *C. elegans* centriole formation. Curr. Biol. 16: 1844–1849.

Fang, G., H. Yu, and M. W. Kirschner, 1998 Direct binding of CDC20 protein family members activates the anaphase-promoting complex in mitosis and G1. Mol. Cell 2: 163–171.

Fay, D. S., S. Keenan, and M. Han, 2002 *fzr-1* and *lin-35/Rb* function redundantly to control cell proliferation in *C. elegans* as revealed by a nonbiased synthetic screen. Genes Dev. 16: 503–517.

Fu, J., I. M. Hagan, and D. M. Glover, 2015 The centrosome and its duplication cycle. Cold Spring Harb. Perspect. Biol. 7: a015800.

García-Higuera, I., E. Manchado, P. Dubus, M. Cañamero, J. Méndez *et al.*, 2008 Genomic stability and tumour suppression by the APC/C cofactor Cdh1. Nat. Cell Biol. 10: 802–811.

Glotzer, M., A. W. Murray, and M. W. Kirschner, 1991 Cyclin is degraded by the ubiquitin pathway. Nature 349: 132–138.

Golden, A., P. L. Sadler, M. R. Wallenfang, J. M. Schumacher, D. R. Hamill *et al.*, 2000 Metaphase to anaphase (*mat*) transition-defective mutants in *Caenorhabditis elegans*. J. Cell Biol. 151: 1469–1482.

Gönczy, P., 2015 Centrosomes and cancer: revisiting a long-standing relationship. Nat. Rev. Cancer 15: 639–652.

Green, R. A., H. L. Kao, A. Audhya, S. Arur, J. R. Mayers *et al.*, 2011 A high-resolution *C. elegans* essential gene network based on phenotypic profiling of a complex tissue. Cell 145: 470–482.

Habedanck, R., Y. D. Stierhof, C. J. Wilkinson, and E. A. Nigg, 2005 The Polo kinase Plk4 functions in centriole duplication. Nat. Cell Biol. 7: 1140–1146.

Hartwell, L. H., and D. Smith, 1985 Altered fidelity of mitotic chromosome transmission in cell cycle mutants of *S. cerevisiae*. Genetics 110: 381–395.

He, J., W. C. Chao, Z. Zhang, J. Yang, N. Cronin *et al.*, 2013 Insights into degron recognition by APC/C coactivators from the structure of an Acm1-Cdh1 complex. Mol. Cell 50: 649–660.

Holland, A. J., W. Lan, S. Niessen, H. Hoover, and D. W. Cleveland, 2010 Polo-like kinase 4 kinase activity limits centrosome overduplication by autoregulating its own stability. J. Cell Biol. 188: 191–198.

Irniger, S., and K. Nasmyth, 1997 The anaphase-promoting complex is required in G1 arrested yeast cells to inhibit B-type cyclin accumulation and to prevent uncontrolled entry into S-phase. J. Cell Sci. 110: 1523–1531.

Kemp, C. A., K. R. Kopish, P. Zipperlen, J. Ahringer, and K. F. O'Connell, 2004 Centrosome maturation and duplication in *C. elegans* require the coiled-coil protein SPD-2. Dev. Cell 6: 511–523.

Kemp, C. A., M. H. Song, M. K. Addepalli, G. Hunter, and K. O'Connell, 2007 Suppressors of *zyg-1* define regulators of centrosome duplication and nuclear association in *Caenorhabditis elegans*. Genetics 176: 95–113.

Kirkham, M., T. Müller-Reichert, K. Oegema, S. Grill, and A. A. Hyman, 2003 SAS-4 is a *C. elegans* centriolar protein that controls centrosome size. Cell 112: 575–587.

Kitagawa, R., E. Law, L. Tang, and A. M. Rose, 2002 The Cdc20 homolog, FZY-1, and its interacting protein, IFY-1, are required for proper chromosome segregation in *Caenorhabditis elegans*. Curr. Biol. 12: 2118–2123.

Kleylein-Sohn, J., J. Westendorf, M. Le Clech, R. Habedanck, Y. D. Stierhof *et al.*, 2007 Plk4-induced centriole biogenesis in human cells. Dev. Cell 13: 190–202.

Kops, G. J., M. van der Voet, M. S. Manak, M. H. van Osch, S. M. Naini *et al.*, 2010 APC16 is a conserved subunit of the anaphase-promoting complex/cyclosome. J. Cell Sci. 123: 1623–1633.

Kraft, C., H. C. Vodermaier, S. Maurer-Stroh, F. Eisenhaber, and J. M. Peters, 2005 The WD40 propeller domain of Cdh1 functions as a destruction box receptor for APC/C substrates. Mol. Cell 18: 543–553.

Kumar, A., S. C. Girimaji, M. R. Duvvari, and S. H. Blanton, 2009 Mutations in STIL, encoding a pericentriolar and centrosomal protein, cause primary microcephaly. Am. J. Hum. Genet. 84: 286–290.

Leidel, S., and P. Gönczy, 2003 SAS-4 is essential for centrosome duplication in *C elegans* and is recruited to daughter centrioles once per cell cycle. Dev. Cell 4: 431–439.

Leidel, S., M. Delattre, L. Cerutti, K. Baumer, and P. Gönczy, 2005 SAS-6 defines a protein family required for centrosome duplication in *C. elegans* and in human cells. Nat. Cell Biol. 7: 115–125.

Levine, M. S., B. Bakker, B. Boeckx, J. Moyett, J. Lu *et al.*, 2017 Centrosome amplification is sufficient to promote spontaneous tumorigenesis in mammals. Dev. Cell 40: 313–322.e5.

Livneh, I., V. Cohen-Kaplan, C. Cohen-Rosenzweig, N. Avni, and A. Ciechanover, 2016 The life cycle of the 26S proteasome: from birth, through regulation and function, and onto its death. Cell Res. 26: 869–885.

Medley, J. C., M. M. Kabara, M. D. Stubenvoll, L. E. DeMeyer, and M. H. Song, 2017 Casein kinase II is required for proper cell division and acts as a negative regulator of centrosome duplication in *Caenorhabditis elegans* embryos. Biol. Open 6: 17–28.

Meghini, F., T. Martins, X. Tait, K. Fujimitsu, H. Yamano *et al.*, 2016 Targeting of Fzr/Cdh1 for timely activation of the APC/C at the centrosome during mitotic exit. Nat. Commun. 7: 12607.

Miller, J. G., Y. Liu, C. W. Williams, H. E. Smith, and K. F. O'Connell, 2016 The E2F–DP1 transcription factor complex regulates centriole duplication in *Caenorhabditis elegans*. G3 6: 709–720.

Nigg, E. A., and T. Stearns, 2011 The centrosome cycle: centriole biogenesis, duplication and inherent asymmetries. Nat. Cell Biol. 13: 1154–1160.

O'Connell, K. F., C. Caron, K. R. Kopish, D. D. Hurd, K. J. Kemphues *et al.*, 2001 The *C. elegans zyg-1* gene encodes a regulator of centrosome duplication with distinct maternal and paternal roles in the embryo. Cell 105: 547–558.

Paix, A., A. Folkmann, D. Rasoloson, and G. Seydoux, 2015 High efficiency, homology-directed genome editing in *Caenorhabditis elegans* using CRISPR-Cas9 ribonucleoprotein complexes. Genetics 201: 47–54.

Pelletier, L., N. Ozlü, E. Hannak, C. Cowan, B. Habermann *et al.*, 2004 The *Caenorhabditis elegans* centrosomal protein SPD-2 is required for both pericentriolar material recruitment and centriole duplication. Curr. Biol. 14: 863–873.

Pelletier, L., E. O'Toole, A. Schwager, A. A. Hyman, and T. Müller-Reichert, 2006 Centriole assembly in *Caenorhabditis elegans*. Nature 444: 619–623.

Peters, J. M., 2006 The anaphase promoting complex/cyclosome: a machine designed to destroy. Nat. Rev. Mol. Cell Biol. 7: 644–656.

Pfleger, C. M., and M. W. Kirschner, 2000 The KEN box: an APC recognition signal distinct from the D box targeted by Cdh1. Genes Dev. 14: 655–665.

Praitis, V., E. Casey, D. Collar, and J. Austin, 2001 Creation of low-copy integrated transgenic lines in *Caenorhabditis elegans*. Genetics 157: 1217–1226.

Prinz, S., E. S. Hwang, R. Visintin, and A. Amon, 1998 The regulation of Cdc20 proteolysis reveals a role for APC components Cdc23 and Cdc27 during S phase and early mitosis. Curr. Biol. 8: 750–760.

Puklowski, A., Y. Homsi, D. Keller, M. May, S. Chauhan *et al.*, 2011 The SCF-FBXW5 E3-ubiquitin ligase is regulated by PLK4 and targets HsSAS-6 to control centrosome duplication. Nat. Cell Biol. 13: 1004–1009.

Raff, J. W., K. Jeffers, and J. Y. Huang, 2002 The roles of Fzy/Cdc20 and Fzr/Cdh1 in regulating the destruction of cyclin B in space and time. J. Cell Biol. 157: 1139–1149.

Rogers, G. C., N. M. Rusan, D. M. Roberts, M. Peifer, and S. L. Rogers, 2009 The SCF Slimb ubiquitin ligase regulates Plk4/Sak levels to block centriole reduplication. J. Cell Biol. 184: 225–239.

Sarov, M., J. I. Murray, K. Schanze, A. Pozniakovski, W. Niu *et al.*, 2012 A genome-scale resource for *in vivo* tag-based protein function exploration in *C. elegans*. Cell 150: 855–866.

Schwab, M., A. S. Lutum, and W. Seufert, 1997 Yeast Hct1 is a regulator of Clb2 cyclin proteolysis. Cell 90: 683–693.

Schwab, M., M. Neutzner, D. Mocker, and W. Seufert, 2001 Yeast Hct1 recognizes the mitotic cyclin Clb2 and other substrates of the ubiquitin ligase APC. EMBO J. 20: 5165–5175.

Shakes, D. C., A. K. Allen, K. M. Albert, and A. Golden, 2011 *emb-1* encodes the APC16 subunit of the *Caenorhabditis elegans* anaphase-promoting complex. Genetics 189: 549–560.

Shirayama, M., W. Zachariae, R. Ciosk, and K. Nasmyth, 1998 The Polo-like kinase Cdc5p and the WD-repeat protein Cdc20p/*fizzy* are regulators and substrates of the anaphase promoting complex in *Saccharomyces cerevisiae*. EMBO J. 17: 1336–1349.

Sigrist, S. J., and C. F. Lehner, 1997 *Drosophila fizzy*-related down-regulates mitotic cyclins and is required for cell proliferation arrest and entry into endocycles. Cell 90: 671–681.

Song, L., and M. Rape, 2008 Reverse the curse–the role of deubiquitination in cell cycle control. Curr. Opin. Cell Biol. 20: 156–163.

Song, L., and M. Rape, 2011 Substrate-specific regulation of ubiquitination by the anaphase-promoting complex. Cell Cycle 10: 52–56.

Song, M. H., L. Aravind, T. Müller-Reichert, and K. F. O'Connell, 2008 The conserved protein SZY-20 opposes the Plk4-related kinase ZYG-1 to limit centrosome size. Dev. Cell 15: 901–912.

Song, M. H., Y. Liu, D. E. Anderson, W. J. Jahng, and K. F. O'Connell, 2011 Protein phosphatase 2A-SUR-6/B55 regulates centriole duplication in *C. elegans* by controlling the levels of centriole assembly factors. Dev. Cell 20: 563–571.

Strnad, P., S. Leidel, T. Vinogradova, U. Euteneuer, A. Khodjakov *et al.*, 2007 Regulated HsSAS-6 levels ensure formation of a single procentriole per centriole during the centrosome duplication cycle. Dev. Cell 13: 203–213.

Stubenvoll, M. D., J. C. Medley, M. Irwin, and M. H. Song, 2016 ATX-2, the *C. elegans* ortholog of human Ataxin-2, regulates centrosome size and microtubule dynamics. PLoS Genet. 12: e1006370.

Sugioka, K., D. R. Hamill, J. B. Lowry, M. E. McNeely, M. Enrick *et al.*, 2017 Centriolar SAS-7 acts upstream of SPD-2 to regulate centriole assembly and pericentriolar material formation. eLife 6: e20353.

Tang, C. J., R. H. Fu, K. S. Wu, W. B. Hsu, and T. K. Tang, 2009 CPAP is a cell-cycle regulated protein that controls centriole length. Nat. Cell Biol. 11: 825–831.

Tang, C. J., S. Y. Lin, W. B. Hsu, Y. N. Lin, C. T. Wu *et al.*, 2011 The human microcephaly protein STIL interacts with CPAP and is required for procentriole formation. EMBO J. 30: 4790–4804.

The, I., S. Ruijtenberg, B. P. Bouchet, A. Cristobal, M. B. Prinsen *et al.*, 2015 Rb and FZR1/Cdh1 determine CDK4/6-cyclin D requirement in *C. elegans* and human cancer cells. Nat. Commun. 6: 5906.

Thornton, B. R., T. M. Ng, M. E. Matyskiela, C. W. Carroll, D. O. Morgan *et al.*, 2006 An architectural map of the anaphase-promoting complex. Genes Dev. 20: 449–460.

Visintin, R., S. Prinz, and A. Amon, 1997 CDC20 and CDH1: a family of substrate-specific activators of APC-dependent proteolysis. Science 278: 460–463.

Zhang, S., L. Chang, C. Alfieri, Z. Zhang, J. Yang *et al.*, 2016 Molecular mechanism of APC/C activation by mitotic phosphorylation. Nature 533: 260–264.

Zhou, Y., Y. P. Ching, R. W. Ng, and D. Y. Jin, 2003 Differential expression, localization and activity of two alternatively spliced isoforms of human APC regulator CDH1. Biochem. J. 374: 349–358.

Zhu, F., S. Lawo, A. Bird, D. Pinchev, A. Ralph *et al.*, 2008 The mammalian SPD-2 ortholog Cep192 regulates centrosome biogenesis. Curr. Biol. 18: 136–141.

Communicating editor: D. Fay